NASA/TM—2007-214834

Oxidation Through Coating Cracks of SiC-Protected Carbon/Carbon

Nathan S. Jacobson and Don J. Roth
Glenn Research Center, Cleveland, Ohio

Richard W. Rauser
University of Toledo, Toledo, Ohio

Donald M. Curry
Johnson Space Center
Houston, Texas

June 2007

NASA STI Program . . . in Profile

Since its founding, NASA has been dedicated to the advancement of aeronautics and space science. The NASA Scientific and Technical Information (STI) program plays a key part in helping NASA maintain this important role.

The NASA STI Program operates under the auspices of the Agency Chief Information Officer. It collects, organizes, provides for archiving, and disseminates NASA's STI. The NASA STI program provides access to the NASA Aeronautics and Space Database and its public interface, the NASA Technical Reports Server, thus providing one of the largest collections of aeronautical and space science STI in the world. Results are published in both non-NASA channels and by NASA in the NASA STI Report Series, which includes the following report types:

- TECHNICAL PUBLICATION. Reports of completed research or a major significant phase of research that present the results of NASA programs and include extensive data or theoretical analysis. Includes compilations of significant scientific and technical data and information deemed to be of continuing reference value. NASA counterpart of peer-reviewed formal professional papers but has less stringent limitations on manuscript length and extent of graphic presentations.

- TECHNICAL MEMORANDUM. Scientific and technical findings that are preliminary or of specialized interest, e.g., quick release reports, working papers, and bibliographies that contain minimal annotation. Does not contain extensive analysis.

- CONTRACTOR REPORT. Scientific and technical findings by NASA-sponsored contractors and grantees.

- CONFERENCE PUBLICATION. Collected papers from scientific and technical conferences, symposia, seminars, or other meetings sponsored or cosponsored by NASA.

- SPECIAL PUBLICATION. Scientific, technical, or historical information from NASA programs, projects, and missions, often concerned with subjects having substantial public interest.

- TECHNICAL TRANSLATION. English-language translations of foreign scientific and technical material pertinent to NASA's mission.

Specialized services also include creating custom thesauri, building customized databases, organizing and publishing research results.

For more information about the NASA STI program, see the following:

- Access the NASA STI program home page at *http://www.sti.nasa.gov*

- E-mail your question via the Internet to *help@sti.nasa.gov*

- Fax your question to the NASA STI Help Desk at 301–621–0134

- Telephone the NASA STI Help Desk at 301–621–0390

- Write to:
  NASA Center for AeroSpace Information (CASI)
  7115 Standard Drive
  Hanover, MD 21076–1320

NASA/TM—2007-214834

Oxidation Through Coating Cracks of SiC-Protected Carbon/Carbon

Nathan S. Jacobson and Don J. Roth
Glenn Research Center, Cleveland, Ohio

Richard W. Rauser
University of Toledo, Toledo, Ohio

Donald M. Curry
Johnson Space Center
Houston, Texas

National Aeronautics and
Space Administration

Glenn Research Center
Cleveland, Ohio 44135

June 2007

Acknowledgments

Helpful discussions with R.A. Rapp, G. Wang, and X. Zheng, formerly of The Ohio State University; T. Parathasarathy of UES, Inc.; and E. Opila of NASA Glenn Research Center are gratefully acknowledged.

Level of Review: This material has been technically reviewed by technical management.

Available from

NASA Center for Aerospace Information
7115 Standard Drive
Hanover, MD 21076–1320

National Technical Information Service
5285 Port Royal Road
Springfield, VA 22161

Available electronically at http://gltrs.grc.nasa.gov

Oxidation Through Coating Cracks of SiC-Protected Carbon/Carbon

Nathan S. Jacobson and Don J. Roth
National Aeronautics and Space Administration
Glenn Research Center
Cleveland, Ohio 44135

Richard W. Rauser
University of Toledo
Toledo, Ohio 43606

Donald M. Curry
National Aeronautics and Space Administration
Johnson Space Center
Houston, Texas 77058

Summary

The oxidation of SiC-protected carbon/carbon through machined slots and naturally occurring craze cracks in the SiC was studied. The slot and crack geometries were characterized, and the subsurface oxidation of the carbon/carbon substrate at temperatures of 1000 to 1300 °C in air was assessed using weight change, x-ray computed tomography, and optical microscopy of sections. Rate constants were derived from these measurements and compared with a two-step diffusion control model of carbon oxidation. Oxidation kinetic measurements on both the specimens with machined slots and with naturally occurring craze cracks showed good agreement with the model.

Introduction

Reinforced Carbon/Carbon

Figure 1 is a schematic of reinforced carbon/carbon (RCC) with a SiC conversion coating used on the Space Shuttle Orbiter nose cap and wing leading edges. The material is made with a two-dimensional layup of carbon-carbon fabric with repeated applications of a liquid carbon precursor to fill voids (ref. 1). The resultant high strength and light weight make it an ideal aerospace material; however, oxidation is a major concern. An oxidation protection system is based on a SiC conversion coating. Because of the difference in coefficient of thermal expansion (CTE) of the SiC coating and carbon/carbon substrate, the SiC coating shrinks more than the underlying carbon/carbon on cooldown from the coating application temperature. This leads to vertical cracks in the coating, and these cracks are pathways for oxygen to reach the carbon/carbon substrate. Actual RCC used on the orbiters contains glass sealants to plug the cracks; however, this work examines carbon/carbon with only SiC.

The crack morphologies in a similar system have been thoroughly characterized in an elegant study by Yurgartis et al. (ref. 2). Both surface (plan) views and section views of the material were taken to obtain information such as crack spacing, crack width, and crack morphology. Such parameters were obtained for RCC in this study and prove critical to modeling oxidation. Buchanan and Little (ref. 3) have also characterized the crack pattern in a range of SiC coatings on carbon/carbon at various deposition conditions.

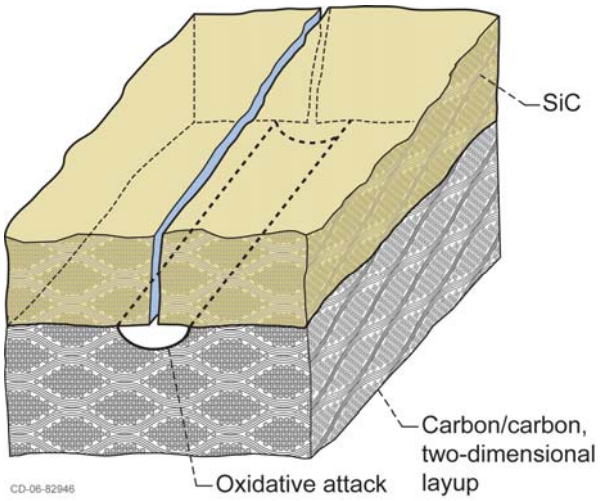

Figure 1.—Reinforced carbon/carbon (RCC) sample.

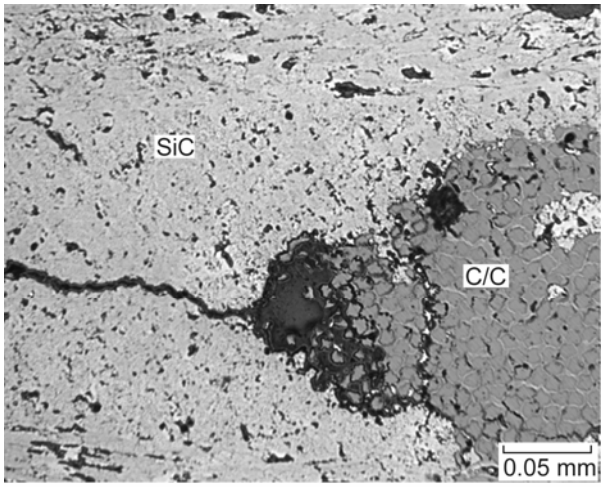

Figure 2.—Optical micrograph showing oxidation void in RCC formed below crack in SiC coating at 1100 °C and 0.0066 atm (667 Pa) for 1 h.

Oxidation Through Coating Cracks

Figure 2 illustrates a typical oxidation void formed because of oxygen diffusion through a coating crack and subsequent reaction. A recent study by the authors outlines the microstructural features which distinguish this void from a processing void (ref. 4). In general, an oxidation void is associated with a path for oxygen ingress (i.e., the crack in fig. 2). At higher temperatures (>1000 °C) these oxidation processes are expected to be diffusion controlled. Diffusion control implies a lack of preferential oxidative attack and hence uniform attack of the carbon/carbon with a plane interface at the void boundary, as illustrated in figure 1. However, a close examination of the void in figure 2 indicates some preferential attack along fiber edges and the resultant "pointed fibers," which are characteristic of reaction control (ref. 5). Thus the actual process is a mix of diffusion and reaction control. It will be shown that diffusion control dominates.

There are numerous studies of carbon oxidation through cracks and fissures in the protective coating and associated models found in the literature. Medford (ref. 6) developed models of oxidation for RCC, assuming pathways for oxygen are the cracks and fissures in SiC. His model encompasses the following processes:

(1) Diffusion of oxygen inward through the cracks and/or fissures in the SiC
(2) Oxidation of SiC crack walls to form SiO_2
(3) Oxidation of carbon/carbon—matrix, fibers, or both
(4) Diffusion of CO outward through the cracks/fissures in the SiC

Medford developed total mass change expressions based on these processes. The expressions were the diffusion equations with modifications for the area of reaction. First he examined the case below 982 °C, where passive oxidation of the SiC is thought to be negligible; then he examined the case above 982 °C, where passive oxidation of the SiC is thought to be significant.

The general process of carbon oxidation in a nonreactive matrix or through a nonreactive coating has been explored by several investigators (refs. 7 to 12). Carbon oxidizes to CO(g):

$$C(s) + \tfrac{1}{2}\, O_2(g) = CO(g) \tag{1}$$

However, thermochemically the equilibrium between O_2, CO, and CO_2 favors the products in the following reaction:

$$\tfrac{1}{2}O_2(g) + CO(g) = CO_2(g) \tag{2}$$

Thus $O_2(g)$ and CO(g) cannot coexist in similar amounts—they immediately will react to form $CO_2(g)$. However, the pairs of species in reaction (2), CO(g) with $CO_2(g)$ and $O_2(g)$ with $CO_2(g)$, may coexist. Thus a two-step oxidation process is required to model carbon oxidation. The two reactions are

1. At the carbon/gas interface:

$$C(s) + CO_2(g) = 2CO(g) \tag{3}$$

Note that $CO_2(g)$ is the oxidizing species.

2. At a distance away from the carbon/gas interface:

$$CO(g) + \tfrac{1}{2}O_2(g) = CO_2(g) \tag{4}$$

In an earlier paper (ref. 12), the authors adapted this two-step diffusion-controlled oxidation model to cylindrical pinholes in the conversion coating. Actual oxidation damage was assessed with weight loss measurements and area measurement of oxidation voids below the pinholes, using cross sections. At 1400 and 1000 °C hemispherical voids were observed on a macroscopic scale, indicating uniform attack and diffusion control. The two-step model described the process reasonably well at 1400 and 1000 °C. However, at 600 °C only minimal oxidation is measured, and reaction control dominated. Hence the model did not fit at this lower temperature.

In the present study, the two-step oxidation model is further extended to describe a half-cylinder trough which forms under a slot or craze crack in the SiC coating. First a series of experiments is performed using machined slots in the coating. This allows testing the model with well-defined oxygen pathway geometry. Then the study is extended to actual through-thickness craze cracks in the coating. Oxidation damage is assessed with cross-sectional views, interrupted or real-time weight loss measurements, and x-ray computed tomography scans. The kinetics of carbon consumption is then compared with the model.

Experimental

Characterization of Slots and Cracks in Test Specimens

The tests described here were done on 1.91-cm-diameter RCC disks with a SiC coating on all sides. These disks were obtained from Lockheed-Martin Missiles and Fire Control in Dallas, Texas. Two sets of experiments were completed. Specimens with machined slots were used for the first set; specimens with naturally occurring craze cracks were used for the second set. Prior to oxidation, both types of specimens were characterized in order to quantify the area of exposed carbon.

In the first set of specimens, artificial craze cracks with well-defined geometries were made with diamond blades (Keen Kut Products, Hayward, CA) of 0.25, 0.51, 0.76, and 1.02 mm thicknesses. These slots were cut to the SiC/carbon-carbon interface. These slotted specimens are shown in figure 3. One slot

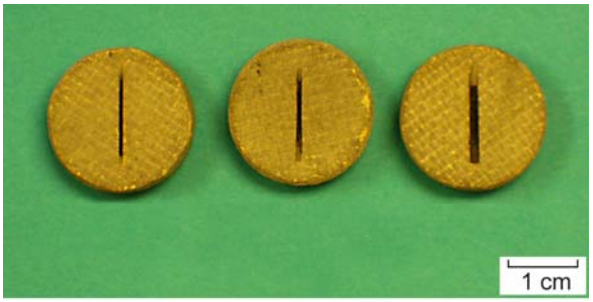

Figure 3.—Machined slots in RCC buttons. From left to right, slots have nominal widths 0.25, 0.51, and 1.02 mm, respectively.

was cut in each specimen where the oxidation kinetics was followed with weight losses; however, two slots of different dimensions were cut in the specimens where the kinetics was followed using microstructure examination and/or x-ray computed tomography. Slot dimensions were carefully measured with a traveling microscope as well as directly from the cross sections and reported in the results section. Total coating thicknesses were measured from cross sections. Because of the variation in coating thickness, 20 random measurements were taken and averaged.

The second set of specimens contained only the naturally occurring craze cracks. These were characterized with techniques similar to Yurgartis et al. (ref. 2). Examination of the surface (plan view) did not reveal the complete crack pattern; however, grinding ~300 μm of SiC clearly revealed the crack pattern, which was then traced, as illustrated in figures 4(a) and (b). Image analysis software (Adobe Photoshop CS2 (Adobe Systems, Inc., San Jose, CA) with Fovea Pro 4.0 (Reindeer Graphics, Asheville, NC)) was used to determine the total crack length per unit area. The view of a section, as shown in figure 5, allowed measurements of crack width at room temperature. Several such sections were examined, and an average of 10 measurements is reported.

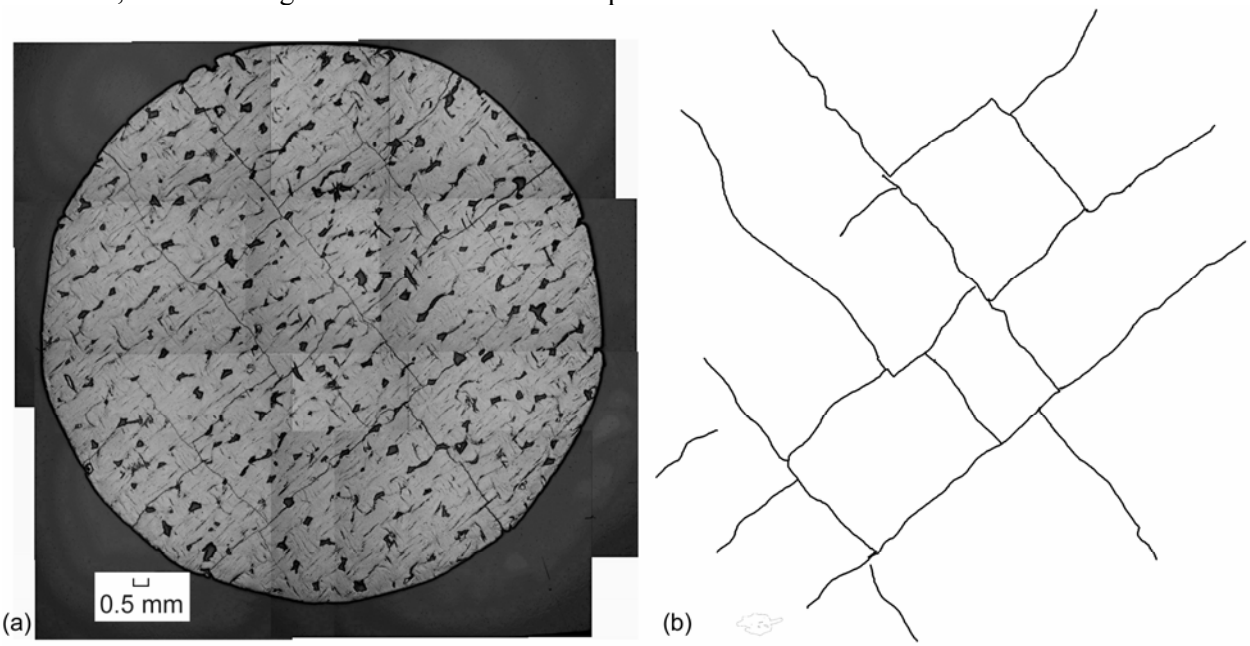

Figure. 4.—Crack pattern on RCC disk. (a) Optical micrograph. (b) “Skeleton” trace of cracks.

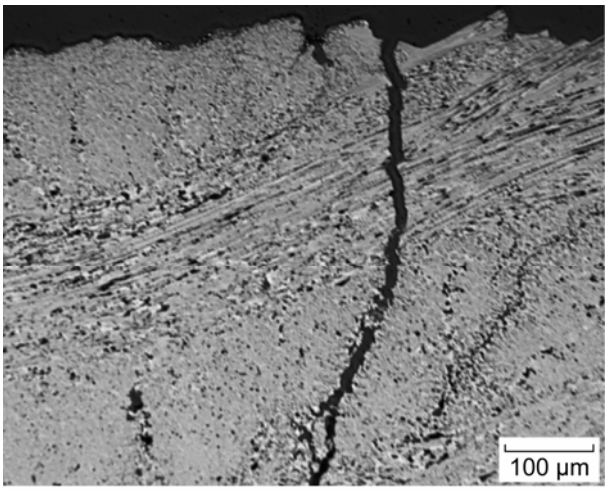

Figure 5.—Crack in SiC conversion coating.

The measured values are listed in table I and compared to the values reported by Yugartis et al. (ref. 2) and Buchanan and Little (ref. 3). "Specimen A" of Yurgartis et al. is SiC-coated carbon/carbon with no matrix inhibitor; "Specimen B" is SiC-coated carbon/carbon with a boron-based matrix inhibitor. It should be noted that the materials examined by Yugartis et al. (ref. 2) and Buchanan and Little (ref. 3) are different from the RCC materials in this study. Here, the RCC had a thicker SiC coating applied by a pack cementation process than the other specimens in which the coating was applied by a chemical vapor deposition process. Yugartis et al. examined cracks that do and do not transverse the entire coating thickness. In this study only through-thickness cracks are examined. Differences in the specific CTE of carbon/carbon and the applied coating would be expected to have a major effect on the crack parameters. Thus the differences listed in table I are not unexpected. It is interesting that despite the differences in crack width and spacing, the ratio of the exposed area of carbon to the surface area of the sample is roughly the same for all materials.

TABLE I.—MEASURED CRACK PARAMETERS FOR SiC-COATED CARBON/CARBON MATERIALS

SiC-coated carbon/carbon material	Coating thickness, mm	Crack length per unit area, mm^{-1}	Crack spacing, mm	Crack width, μm	Crack area per unit area
Present study, RCC	0.78±0.14	0.33±0.04	3.4±0.9	12.8±1.41	4.2×10^{-3}
Yurgartis et al. (ref. 2), Specimen A	0.3024±0.03866	2.985	0.6247±0.2233[a]	1.72±1.41	5.1×10^{-3}
Yurgartis et al. (ref. 2), Specimen B	0.2788±0.02853	3.555	0.6517±0.3356[a]	2.02±1.47	7.3×10^{-3}
Buchanan and Little (ref. 3)	----	----	----	----	$(3–8)\times10^{-4}$

[a]Through coating thickness.

Oxidation Treatments and Sample Analyses

The samples were oxidized in air in either a box furnace or a vertical tube furnace. The kinetics of the box furnace exposures were followed with weight measurements every 0.5 h for a total of 2.5 h at 1200 °C. The craze crack specimens were suspended from a Cahn C–1000 (Cahn Instruments, Cerritos, CA) recording electrobalance by a sapphire fiber with a platinum wire basket into the vertical tube furnace. To avoid platinum silicide formation, the platinum wire was lined with alumina beads. Bottled air at 1 atm (101 325 Pa) was used at a flow rate of 1.67×10^{-3} liter/s, and isothermal oxidation tests were performed at 1000, 1100, 1200, and 1300 °C.

Selected samples were mounted and sectioned for optical microscopy to obtain measurements of oxidation void size. A specialized sample preparation procedure involved a premount of the entire sample in epoxy. A standard vacuum infiltration was done followed by a high-pressure application to fill the open porosity. Then the sample was sectioned, remounted in a standard metallographic mold, and polished with diamond pastes. This ensured clear microstructures and preserved the interface between the SiC and the carbon/carbon.

X-ray computed tomography (CT) was used to provide additional images of the oxidation damage, without sectioning. This SmartScan Model 100 (CITA Systems, Inc., Pueblo, CA) system utilizes a Feinfocus FXE–160 (COMET AG, Flamatt, Switzerland) microfocus x-ray source to produce very high-resolution imaging of samples, approaching 25 μm, in the CT mode of operation. The major hardware components of this system included the x-ray source, an area detector system, a five-axis object positioning subassembly, and a lead-lined radiation cabinet. A dual-processor computer system controlled the data acquisition and image processing. The slice plane thickness was 120 μm per slice for these samples. Putting together slices electronically gave a three-dimensional view of oxidation damage.

Oxidation Model Adapted to Slots and Cracks

Figure 6 is a schematic of the two-step diffusion-controlled model for oxidation through a pore or crack. Note that CO_2 is the oxidizer and reaction (3) occurs at position $x = 0$ whereas reaction (4) occurs

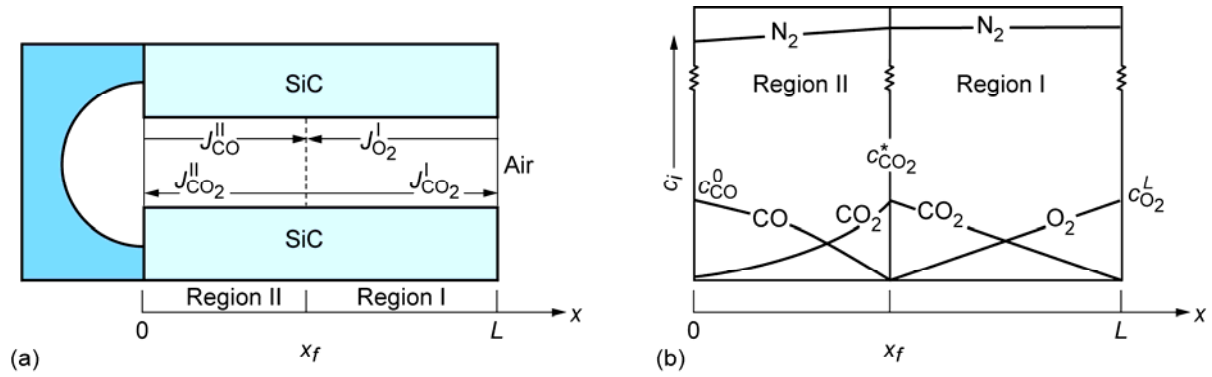

Figure 6.—Two-step diffusion control model (ref. 12). (a) Schematic of fluxes and boundaries. (b) Relative concentrations of gases.

at position $x = x_f$. A list of symbols used in this report is in the appendix to aid the reader.

The molar flux, J_i, of each species, i, is defined by

$$J_i = D_i^{\text{eff}}\left(\frac{\partial c_i}{\partial x}\right) + v_i^{\text{ave}} c_i \tag{5}$$

The first term is the diffusive term and the second is the convective term. Here $D_{i,\text{eff}}$ is the effective gas phase diffusivity, c_i is the molar concentration of species i (i = CO, CO_2, or O_2), and x is the distance down the slot or crack. The average molar velocity v_i^{ave} is defined as

$$v_i^{\text{ave}} = \frac{\sum_i c_i v_i}{\sum_i c_i} = \frac{\sum_i J_i}{c_T} \tag{6}$$

Here c_T is the sum of concentrations. Equation (5) becomes

$$J_i = D_i^{eff}\left(\frac{\partial c_i}{\partial x}\right) + \frac{c_i}{c_T}\sum_i J_i \tag{7}$$

The boundary conditions are shown in figure 6(b):

$$\text{At } x = 0: \quad c_{CO} = c^0_{CO} \quad c_{CO_2} = c^0_{CO_2}$$

$$\text{At } x = x_f: \quad c_{CO_2} = c^*_{CO_2} \quad c_{O_2} = c_{CO} = 0 \tag{8}$$

$$\text{At } x = L: \quad c_{O_2} = c^L_{O_2} \quad c_{CO_2} = 0$$

As shown in figure 6(b) L is the total crack depth, which is the coating thickness.
Consider the fluxes in Region 1 (fig. 6(a)). Here $J^{\text{I}}_{O_2} = -J^{\text{I}}_{CO_2}$ and hence the convective term in equation (7) is zero. The fluxes of O_2(g) and CO_2(g) in this region are thus calculated as

$$J^{\mathrm{I}}_{\mathrm{O}_2} = -D_{\mathrm{O}_2}\left(\frac{\partial c_{\mathrm{O}_2}}{\partial x}\right) = \frac{-D_{\mathrm{O}_2} c^{L}_{\mathrm{O}_2}}{\left(L - x_f\right)} \tag{9a}$$

$$J^{\mathrm{I}}_{\mathrm{CO}_2} = D_{\mathrm{CO}_2}\left(\frac{\partial c_{\mathrm{CO}_2}}{\partial x}\right) = \frac{D_{\mathrm{CO}_2} c^{*}_{\mathrm{CO}_2}}{\left(L - x_f\right)} \tag{9b}$$

A determination of the CO_2 flux emerging from the crack or slot, $J^{\mathrm{I}}_{\mathrm{CO}_2}$, is the ultimate goal, because it is a measure of carbon consumption. First the quantity x_f is needed. This can only be obtained as the ratio x_f/L, which is derived from the following equations (eqs. (10) to (17)). The two fluxes in equation (9) are equal and opposite. From this fact, one can deduce the concentration gradients in figure 6(b). The concentration of CO_2 at $x = x_f$ is

$$c^{*}_{\mathrm{CO}_2} = \frac{D_{O_2} c^{L}_{\mathrm{O}_2}}{D_{\mathrm{CO}_2}} \tag{10}$$

Equation (7) for CO and CO_2 in Region II (fig. 6(a)) is more complex, as now there is a convection term since the stoichiometry of reaction (3) requires

$$J^{\mathrm{II}}_{\mathrm{CO}} = -2J^{\mathrm{II}}_{\mathrm{CO}_2} \tag{11}$$

Thus equation (7) for CO_2 becomes

$$J^{\mathrm{II}}_{\mathrm{CO}_2} = -D_{\mathrm{CO}_2}\left(\frac{\partial c_{\mathrm{CO}_2}}{\partial x}\right) - \frac{c_{\mathrm{CO}_2} J^{\mathrm{II}}_{\mathrm{CO}_2}}{c_T} \tag{12}$$

Rearranging to separate variables gives

$$J^{\mathrm{II}}_{\mathrm{CO}_2}\,\mathrm{d}x = -D_{\mathrm{CO}_2}\left(\frac{c_T}{c_T + c_{\mathrm{CO}_2}}\right)\mathrm{d}c_{\mathrm{CO}_2} \tag{13}$$

This can be integrated from $c_{\mathrm{CO}_2} = c^{*}_{\mathrm{CO}_2}$ at $x = x_f$ and $c_{\mathrm{CO}_2} = c^{0}_{\mathrm{CO}_2}$ at $x = 0$:

$$J^{\mathrm{II}}_{\mathrm{CO}_2} = \frac{-D_{\mathrm{CO}_2} c_T}{x_f} \ln\left(\frac{c_T + c^{*}_{\mathrm{CO}_2}}{c_T + c^{0}_{\mathrm{CO}_2}}\right) \tag{14}$$

This can be simplified further using equation (10) and the fact that $c^{*}_{\mathrm{CO}_2} >> c^{0}_{\mathrm{CO}_2}$:

$$J^{\mathrm{II}}_{\mathrm{CO}_2} = \frac{-D_{\mathrm{CO}_2} c_T}{x_f} \ln\left(1 + \frac{D_{\mathrm{O}_2} c^{L}_{\mathrm{O}_2}}{D_{\mathrm{CO}_2} c_T}\right) \tag{15}$$

A mass balance between CO and O_2 gives

$$J_{CO}^{II} = -2J_{O_2}^{I} \tag{16}$$

Combining this with equation (11),

$$J_{CO_2}^{II} = J_{O_2}^{I} \tag{17}$$

When equation (15) is combined with equations (17) and (9a),

$$J_{CO_2}^{II} = \frac{-D_{O_2}c_{O_2}^{L}}{\left(L - x_f\right)} = \frac{-D_{CO_2}c_T}{x_f}\ln\left(1 + \frac{D_{O_2}c_{O_2}^{L}}{D_{CO_2}c_T}\right) \tag{18}$$

Solving for L/x_f gives

$$\frac{L}{x_f} = 1 + \frac{D_{CO_2}c_{O_2}^{L}}{D_{O_2}c_T}\left[\ln\left(1 + \frac{D_{O_2}c_{O_2}^{L}}{D_{CO_2}c_T}\right)\right]^{-1} \tag{19}$$

Next the gas phase diffusivities, D_{i,N_2}, of O_2 in N_2 and CO_2 in N_2 must be estimated. This is done with the Chapman-Enskog correlation (ref. 13), which yields diffusivity in cm^2/s when the variables in the expression below are expressed in the appropriate units:

$$D_{i,N_2} = 0.0018583\left(\frac{1}{M_i} + \frac{1}{M_{N_2}}\right)^{1/2} T^{3/2}\left(\frac{1}{P\sigma_{i,N_2}^2\Omega}\right) \tag{20}$$

Here M_i is the molecular weight (g/mol) of species i, T is the absolute temperature (K), P is the pressure (atm), σ_{i,N_2} is the average of the molecular diameter (Å) of species i and N_2, and Ω_{i,N_2} is the collision integral (unitless). The later two were determined from the tables of Svehla (ref. 14) and Sherwood et al. (ref. 15). Table II lists some calculated diffusivities. The value of L/x_f is also shown in table II and is constant with temperature.

TABLE II.—DIFFUSIVITIES OF O_2(g) AND CO_2(g) IN N_2(g) AND POSITION OF BOUNDARY BETWEEN REGIONS I AND II (FIG. 6(a)). [Total pressure is 1 atm (101 325 Pa).]

Temperature, °C	D_{O_2,N_2}, cm^2/s	D_{CO_2,N_2}, cm^2/s	L/x_f
1000	2.38	1.86	2.13
1100	2.70	2.11	2.13
1200	3.03	2.38	2.13
1300	3.38	2.65	2.13

For narrow cracks, the contribution of Knudsen diffusion must also be considered. In the Knudsen diffusion regime, molecule-wall collisions dominate over molecule-molecule collisions. The effective diffusivity, D^{eff}, is a combination of the ordinary diffusivity, D^{ord}, and Knudsen diffusivity, D^K. The Knudsen diffusivity can be estimated for a pore as (ref. 16)

$$D_i^k = (9.7)\left(10^3\right) q \sqrt{\frac{T}{M_i}} \tag{21}$$

Here q is the pore radius in centimeters. Equation (21) is for a pore, not a crack, but it is still suitable for this general discussion of Knudsen effects. The combined effects of ordinary and Knudsen diffusion can be written as (ref. 17)

$$\frac{1}{D^{\text{eff}}} = \frac{1}{D^{\text{ord}}} + \frac{1}{D^k} \tag{22}$$

When the mean free path is greater than 10 crack widths, then Knudsen diffusion is the dominating flow mechanism (ref. 18). For the 1 atm total pressure used in this study, the mean free path is ~3.3×10^{-7} m. The machined slots are much larger than this, and even the craze cracks (~1.28×10^{-5} m) are larger than the mean free path. This becomes apparent by comparing $D^{\text{ord}}/D^{\text{eff}}$ to the pore diameter, as shown in figure 7. The level parts of the plots show $D^{\text{eff}} = D^{\text{ord}}$. At the 1 atm (101 325 Pa) pressure used in this study, the average crack width indicates a very small Knudsen contribution; however, at lower pressures which are closer to actual reentry pressure, the Knudsen contribution must be considered.

Now with values for x_f/L and the gas phase diffusivities carbon consumption can be calculated. As noted, this is simply the molar flux of CO_2(g) emerging from the crack, as given by equations (9b) and (9a):

$$J^{\text{I}}_{\text{CO}_2} = \frac{D_{\text{CO}_2} c^*_{\text{CO}_2}}{\left(L - x_f\right)} = \frac{D_{\text{O}_2} c^L_{\text{O}_2}}{L\left[1 - \left(\frac{x_f}{L}\right)\right]} \tag{23}$$

The denominator is written in the above form, since x_f/L is now a known quantity. The goal is to estimate the radius of the cavity formed below a crack, as shown in figure 6.

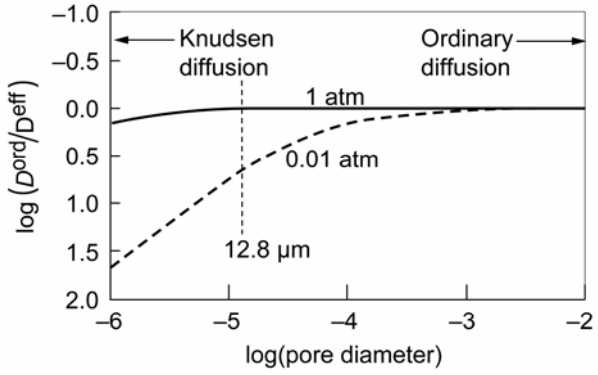

Figure 7.—Plot to show relative contribution of Knudsen diffusivity to effective diffusivity. The vertical line shows average crack width.

The flux of CO_2(g) (eq. (11)) can be converted to a mass loss of carbon as

$$\frac{dW_C}{dt} = M_C J^I_{CO_2} wl = \frac{M_C D_{O_2} P_{O_2} wl}{RTL\left[1-\left(\frac{x_f}{L}\right)\right]} \tag{24}$$

Here W_C is the weight loss of carbon, M_C is the molecular weight of carbon (12 gm/mol), R is the gas constant, w is the crack width, and l is the crack length. Note that the wl term would be omitted for weight loss per unit area.

The weight loss with time can be related to the volume change with time of the cavity at the base of the crack. Assume a rectangular crack with a half-cylinder cavity of radius r growing at its base. In practice the nonideality of the crack is accounted for with a "tortuosity factor" (ref. 19). For this approximation a tortuosity factor of 1 is assumed.

The weight loss can be related to the radius of the growing half-cylinder cavity as

$$\frac{dW_C}{dt} = \rho\frac{dV}{dt} = \rho\left[\frac{d\left(\frac{\pi r^2 l}{2}\right)}{dt}\right] \tag{25}$$

Here r is the radius of the half cylinder and ρ is the density of carbon/carbon taken to be 1.362 g/cm^3 (ref. 20). Equating equations (24) and (25) and separating variables gives

$$d\left(\frac{\pi r^2 l}{2}\right) = \frac{M_C D_{O_2} P_{O_2} wl\, dt}{\rho RTL\left[1-\left(\frac{x_f}{L}\right)\right]} \tag{26}$$

Integrating and solving for r results in the following:

$$r = \sqrt{\frac{2M_C D_{O_2} P_{O_2} wt}{\pi\rho RTL\left[1-\left(\frac{x_f}{L}\right)\right]}} \tag{27}$$

Note the crack length cancels out and does not appear in the final expression. Equations (24) and (27) are the key equations used to calculate oxidation damage in subsequent sections.

An important consideration is the variation of the crack width with temperature. This is minor for the machined slots, but significant for the craze cracks. The actual coating is not dense SiC, but rather converted carbon-carbon fibers and carbon matrix material. For this approximation the accepted coefficient of thermal expansion (CTE) for SiC as ~6.1×10^{-6} K^{-1} is used (ref. 21). The thermal expansion along a carbon fiber is taken as 1×10^{-6} K^{-1} (ref. 22). This puts the coating in tension on cooldown, which leads to the cracks during processing. However, it leads to compression and possible crack closing during heatup to temperatures above the processing temperature. The extent of crack closure can be estimated as

$$W_{RT} = \Delta\alpha s(T_P - T) \tag{28}$$

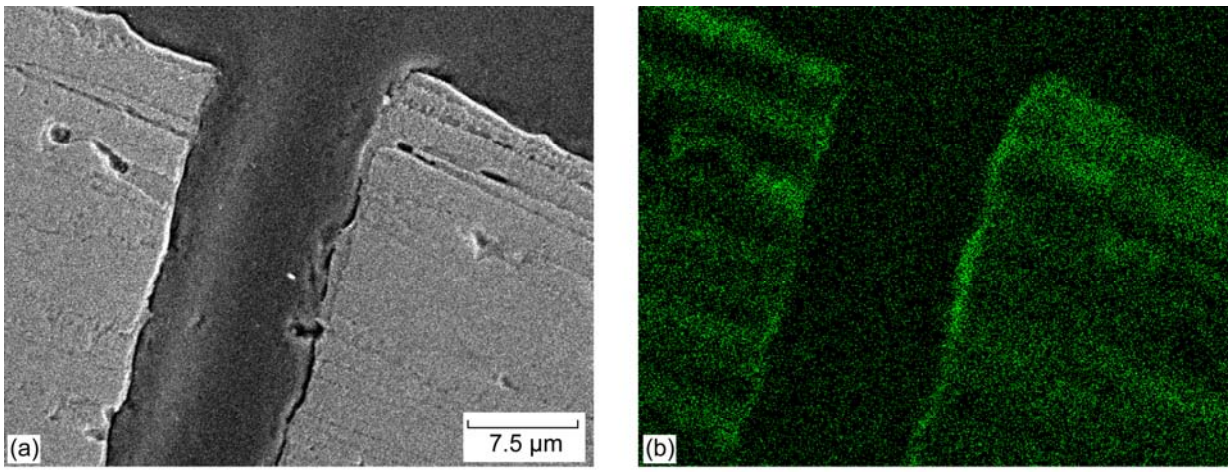

Figure 8.—Oxide film on surface of SiC coating (0.5 h in air at 1200 °C) at crack opening. (a) Electron micrograph. (b) Oxygen map.

Here W_{RT} is the crack width at room temperature, Δα is the difference between the CTE of SiC and that of the carbon/carbon, s is the crack spacing, T_P is the processing temperature (taken as ~1650 °C), and T is the operating temperature. Since the crack width at room temperature is 12.8±1.4 μm, the crack spacing is calculated to be 1.5±0.2 mm from the equation above, reasonably close to that measured given the approximation of the CTEs. This calculated crack spacing is used in the above equation to estimate crack width at the oxidation temperature. At 1200 °C the crack width was calculated to be 7.1 μm.

Oxidation along the SiC crack wall may affect the rate of carbon/carbon oxidation. As will be discussed, the samples gain considerable weight due to passive oxidation. Microscopy indicates that thin films of SiO_2 form on both the internal and external surfaces of the SiC coating. Figure 8 shows the mouth of a crack and only a thin (~0.25-μm) film of SiO_2.

On the basis of the thin films of oxide observed, the oxidation rate constants for high-purity chemically vapor deposited (CVD) SiC (ref. 23) are used. The results shown in table III are somewhat lower than the thicknesses of the oxide film on both the slots and cracks. It is probable the lower purity SiC in the conversion coating has an oxidation rate constant of an order of magnitude or so greater than that of CVD SiC. Such behavior is well documented (ref. 24). Nonetheless images such as those in figure 8 indicate that under the conditions of this study, crack closure due to wall oxidation can be neglected.

TABLE III.—ESTIMATED OXIDE FILM THICKNESSES ON SLOT OR CRACK WALLS OF SiC COATING

Temperature, °C	Rate constant		Oxide thickness	
	1 atm O_2,[a] $\mu m^2/h$	0.21 atm O_2, $\mu m^2/h$	0.5 h in 0.21 atm O_2, μm	2.5 h in 0.21 atm O_2, μm
1200	1.82×10^{-2}	3.78×10^{-3}	4.35×10^{-2}	9.72×10^{-2}
1300	3.76×10^{-2}	7.90×10^{-3}	6.28×10^{-2}	0.14

[a]From reference 23.

Results and Discussion: Measured Oxidation Kinetics and Comparison With Model

Oxidation Below Machined Slots in SiC Coating

Initially, two specimens were oxidized at 1200 °C and examined with both CT and optical microscopy. One specimen had nominal 0.25- and 0.51-mm slots machined in the face. The other specimen had nominal 0.76- and 1.01-mm slots machined in the face. Cross-sectional micrographs for the cavities formed below the nominal 0.25-mm slots are shown in figures 9(a) and (b). Oxidation damage below all slots exhibited this type of half-cylinder morphology. Figures 10(a) and (b) show the x-ray CT information.

The data in figures 9 and 10 make several important points. The similarity between the CT images and the actual optical microscopy images give credibility to the use of CT imaging to precisely size and characterize the three-dimensional morphology of this type of oxidation damage (ref. 25). Both the optical microscope images and the CT images indicated the oxidation damage occurs in the form of a half cylinder. On a macroscopic scale this indicates even attack in all directions, supporting diffusion control of the oxidation process and the use of a half cylinder in the model.

Using image analysis software the areas of the oxidation cavities were measured. Approximating these areas as semicircles allows calculation of effective radii. The experimental results are compared to the predictions from equation (27) in table IV. The error in the predicted oxidation slot radius values is due to uncertainty in the measurement of the slot widths. Agreement between the measured and predicted cavity radius is within a factor of 0.45 to 0.62. All the measurements are consistently lower than the predictions, which is likely due to carbon consumption beyond the apparent boundaries of the half cylinder, as seen clearly in figure 9(b).

TABLE IV.—MEASURED AND CALCULATED RADII OF OXIDATION CAVITY FOR SiC-COATED RCC SPECIMENS WITH MACHINED SLOTS
[In static air at 1200 °C.]

Width of slot, mm	Measured radius, mm	Calculated radius,[a] r, mm
0.5 h exposure		
0.26±0.02	0.99±0.07	1.82±0.07
0.53±0.02	1.22±0.03	2.60±0.05
0.81±0.02	1.51±0.03	3.32±0.04
1.08±0.01	1.51±0.03	3.77±0.02
2.5 h exposure		
0.44±0.08	2.38±0.01	3.80±0.30
0.59±0.08	2.60±0.16	4.40±0.26
1.05±0.07	2.96±0.04	5.87±0.20

[a]From equation (27).

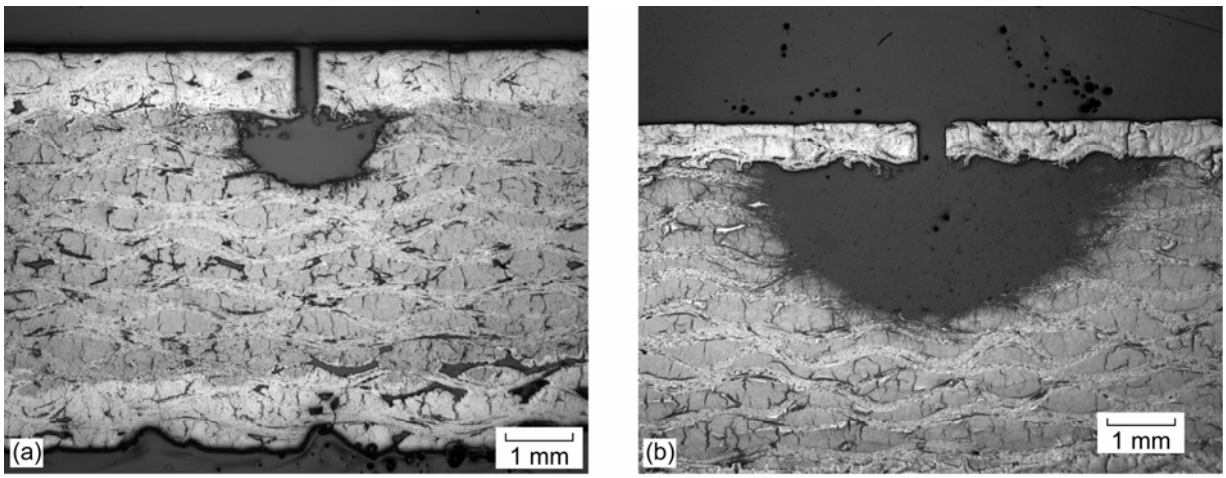

Figure 9.—Oxidation below nominal 0.25-mm slots in SiC coating. (a) 0.28-mm slot in air at 1200 °C for 0.5 h. (b) 0.37-mm slot in air at 1200 °C for 2.5 h.

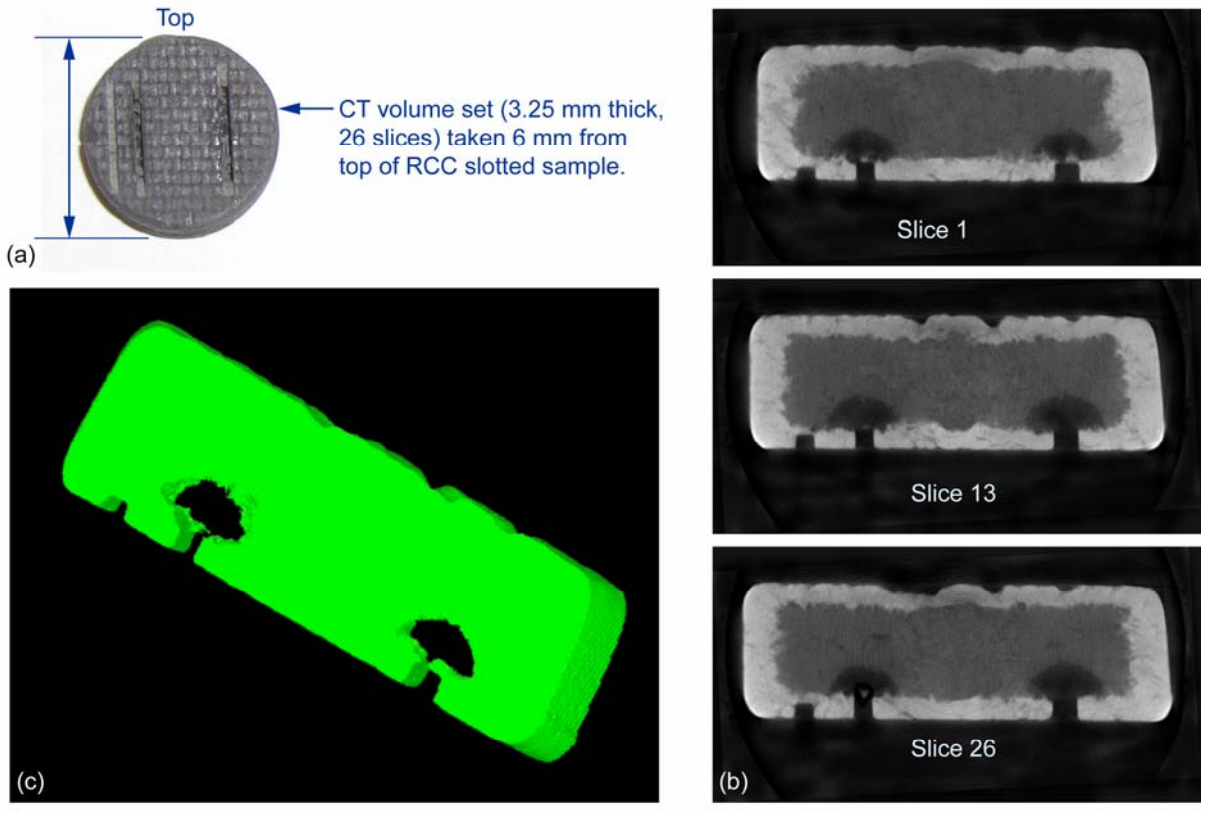

Figure 10.—X-ray computed tomography (CT) of machine-slotted SiC-coated RCC oxidized for 0.5 h in air at 1200 °C. (a) Approximate CT sample locations. (b) Three CT slices. Slot near notch on left is 0.76 mm, and slot on right is 1.03 mm. (c) Three-dimensional reconstruction of disk.

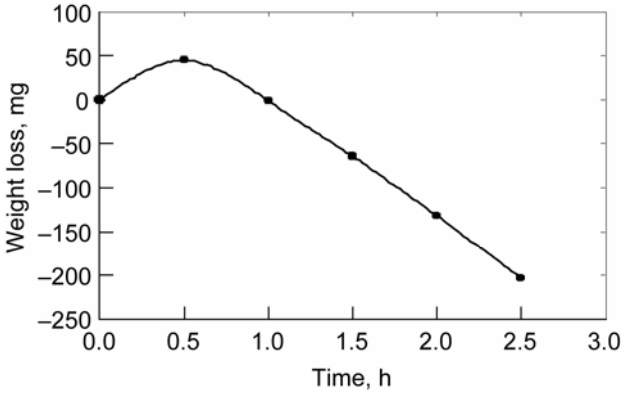

Figure 11.—Oxidation kinetics determined from interrupted weight loss measurements for RCC specimen with 0.484-mm slot width at 1200 °C in air.

A second set of experiments was done to follow the kinetics of oxidation below machined slots with weight loss as the indicator of oxidation damage. In this case specimens with only a single slot were used. Kinetics were followed using interrupted weight loss measurements. A typical kinetic curve is shown in figure 11. Note there is an initial weight gain, which is likely passive oxidation of the SiC, followed by a weight loss. The passive oxidation of the SiC will be discussed in the following section. The rates of weight loss are the carbon oxidation rates per the exposed area of carbon, which was determined from the slot dimensions. Table V compares the measured rates with those predicted. Rates are normalized per unit area of exposed carbon, and hence the predictions are all the same for the given temperature of 1200 °C. The error in the predicted oxidation rate values is due to uncertainty in the measurement of slot depth (coating thickness). The error in the measured rate values is due to uncertainty in the measurements of slot width and length. Note that these errors make the measured rates for three of the four smaller slots within the limits of the predictions (table V). For the larger width slots (~1 mm), the measured rates are ~0.33 of the predicted. The reasons for this are not clear.

TABLE V.—OXIDATION RATES FOR SiC-COATED RCC SPECIMENS WITH MACHINED SLOTS

[At T = 1200 °C in air.]

Slot width, w, mm	Slot length, l, mm	Weight loss rate, mg/h·mm^2	
		Measured	Calculated[a]
0.484±0.062	8.177±0.923	34±6	55±10
0.312±0.033	8.284±0.63	48±6	55±10
0.560±0.013	7.094±0.132	48±1	55±10
0.466±0.04	7.114±0.019	57±5	55±10
1.116±0.024	7.602±0.101	18±1	55±10
0.963±0.0041	7.624±0.039	21±1	55±10

[a]From equation (24).

Oxidation Below Craze Cracks in the SiC Coating

Having established the validity of the model with the machined slots, it is now appropriate to proceed to the more realistic situation of craze cracks in the SiC coating. Now there is a less well-defined geometry, as illustrated with the crack pattern in figure 4 and crack width measurement in figure 5. Nonetheless these measurements can be used to estimate approximate values for the diffusion model.

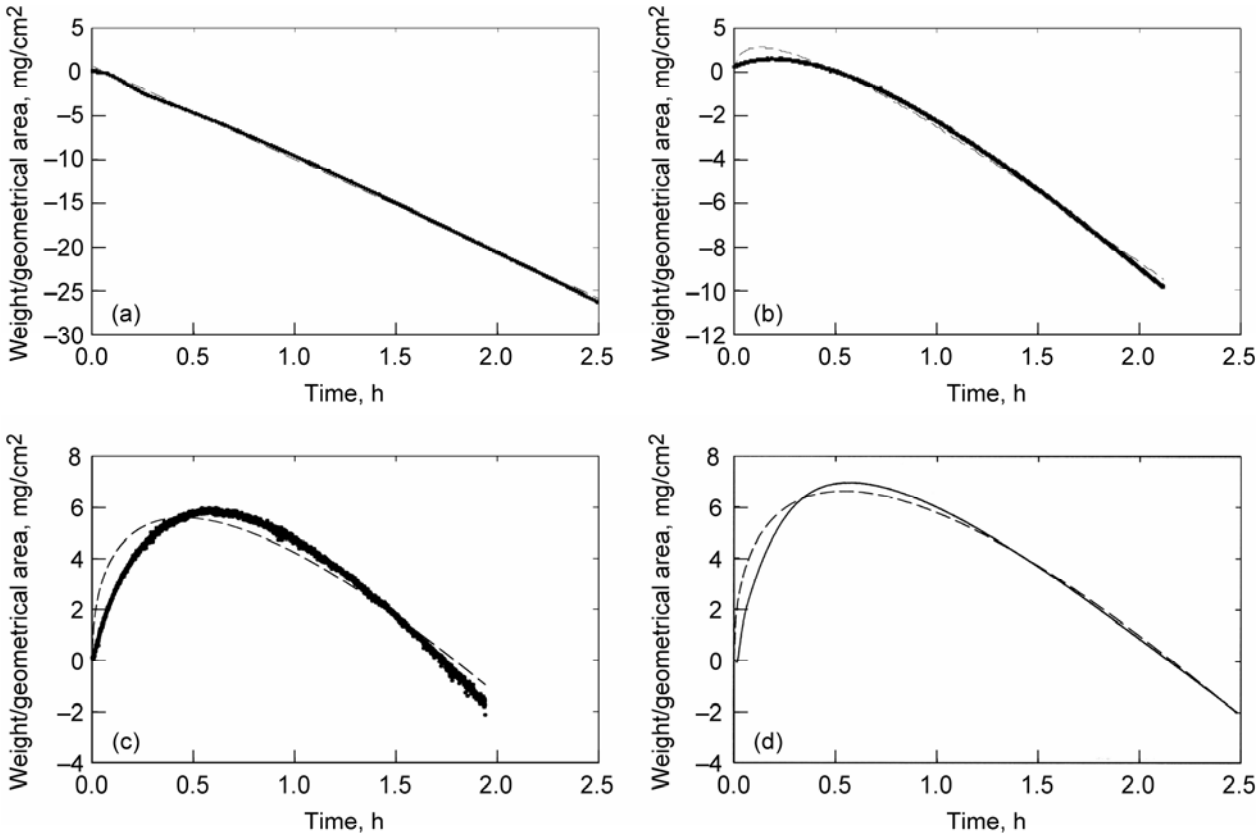

Figure 12.—Oxidation kinetics for RCC in air at 1 atm (101 325 Pa) and 100 cm^3/min flow rate. (a) 1000 °C. (b) 1100 °C. (c) 1200 °C. (d) 1300 °C.

Oxidation kinetics for these specimens were followed with a recording thermobalance that enabled continuous weight change measurements. Results for 1000, 1100, 1200, and 1300 °C are given in figures 12(a) to (d). These data are reported in weight change per geometrical surface area. As will be discussed, the geometric surface area must be modified for actual reactive area of oxidation, which is different for each of the two processes occurring.

The oxidation kinetics suggest a combined parabolic/linear rate law. The initial weight gain observed at the three higher temperatures is likely due to the passive oxidation of SiC, which is parabolic:

$$\left(\frac{\Delta M}{A}\right) = \sqrt{k_p t} \tag{29}$$

Here $\left(\frac{\Delta M}{A}\right)$ is the specific weight change (weight per unit area), k_p is the parabolic rate constant, and t is the time. The specific weight change over the surface area A of the SiC is taken as the geometric area of the sample disk. The weight loss after ~0.5 h is linear with time and most likely due to carbon oxidation through the craze cracks. It is described by

$$\left(\frac{\Delta M}{A'}\right) = k_l t \tag{30}$$

Here k_l is the linear rate constant. Note that A' is the exposed area of carbon/carbon. This is the crack width at temperature multiplied by the total crack length for a particular sample.

The changes in the kinetic curves with temperature support the interpretation of the process as passive SiC oxidation coupled with C/C oxidation. At 1000 °C the initial parabolic regime was not observed; however, at 1200 and 1300 °C it was quite evident. This is due to the fact that passive oxidation of SiC shows a strong dependence on temperature (ref. 23). Note, however, that the linear rate constant is relatively temperature independent. Diffusion-controlled oxidation of carbon shows only a weak temperature dependence, a combination of the $T^{1/2}$ dependence of the diffusion coefficient and the T^1 dependence of the crack closure due to thermal expansion. This dependence may not be evident in the limited data set in this study.

The combined passive oxidation of SiC/linear oxidation of carbon rate law is written as

$$\left(\frac{\Delta M}{A}\right)_{\text{total}} = \sqrt{k_p t} + k_l t \tag{31}$$

Here $\left(\frac{\Delta M}{A}\right)_{\text{total}}$ is the measured weight change per unit of geometrical area, k_p is the parabolic rate constant, t is the time, and k_l is the linear rate constant. This expression is similar to that used to describe the combined oxidation/vaporization of chromium alloys (ref. 26) and SiC (ref. 27), but this is somewhat simpler in that there are two independent processes occurring.

The dashed lines in figures 12(a) to (d) are fits of equation (31) to each kinetic curve. From these fits the parabolic and linear rate constants can be derived. Fits to the linear region are good; fits to the parabolic region are only approximate because of such factors as changing surface areas of passive oxidation and passive oxidation internal to the coating, which are not included in equation (31). The parabolic and linear rate constants extracted from the fit to the kinetic data are given in table VI. The parabolic rate constant was taken directly from the fit. Note that the listed parabolic rate constants are many orders of magnitude greater than those measured for high-purity SiC (ref. 23). This is due to extensive internal oxidation of the porous SiC conversion coating. Measurements of the SiC conversion coating density have been reported to be 2.114 g/cm^3 (ref. 20). When compared with the theoretical density of 3.217 g/cm^3 for SiC, this indicates a high amount of porosity. This porosity leads to the large extent of internal oxidation.

TABLE VI.— MEASURED AND CALCULATED RATES OF RCC OXIDATION THROUGH CRAZE CRACKS

Sample temperature, °C	Geometrical surface area, mm^2	Total crack length,[a] mm	Crack width, μm	Area of carbon exposed by craze cracks,[b] mm^2	Calculated linear rate,[c] mg/mm^2·hr	Measured linear rate,[c,d] mg/mm^2·hr	Measured parabolic rate,[e] mg^2/mm^4·hr
Room temperature			12.8±1.4				
1000	850.2±10	281±34	10.2±2.7	2.87±0.8	50±9	31±9	-----
1100	935.5±10	309±37	8.7±2.3	2.67±0.8	53±9	31±9	3.94×10^{-3}
1200	946.8±10	312±37	7.1±1.8	2.21±0.6	55±10	53±15	2.79×10^{-2}
1300	940.2±10	310±37	5.5±1.4	1.71±0.5	57±10	67±20	3.25×10^{-2}

[a]Equal to (geometrical area × crack length)/unit area.
[b]Equal to (total crack length) × (crack width).
[c]From equation (24).
[d]Area is exposed area of carbon/carbon.
[e]Area is geometrical surface area.

The linear rate constant shown in table VI was taken from the fit and multiplied by the geometrical surface area. This gives a rate of carbon oxidation per area of exposed carbon/carbon and allows direct comparison to the calculated rate in table VI. The predicted rates were obtained from equation (24).

The cracks in the SiC form a complex geometry. The oxidation cavities are an irregular shape as seen in the micrograph in figure 2. Figure 13(a) shows the location of two CT scans, and figure 13(b) shows the results of the CT scans illustrating the varying size and shape of the oxidation cavity below a craze crack. The actual oxidation cavities are darker and are outlined in white in figure 13(b).

Despite this complex geometry of both the craze crack and the resultant oxidation damage, average values of crack width and length can be put into the oxidation model to estimate the rates. These are shown in table VI. Experimental rates were found to be both greater and less than the predicted rates for the temperature range of 1000 to 1300 °C. As in the case of the slots, the error associated with the predicted oxidation rate values is due to variation in the measurement of crack depth (coating thickness), and error associated with the measured rate values is primarily due to uncertainty in the crack length and width measurements. The predicted and measured rates show agreement within experimental error, which is remarkable given the irregular geometry of the cracks and corresponding oxidation damage as well as the approximations used in this study.

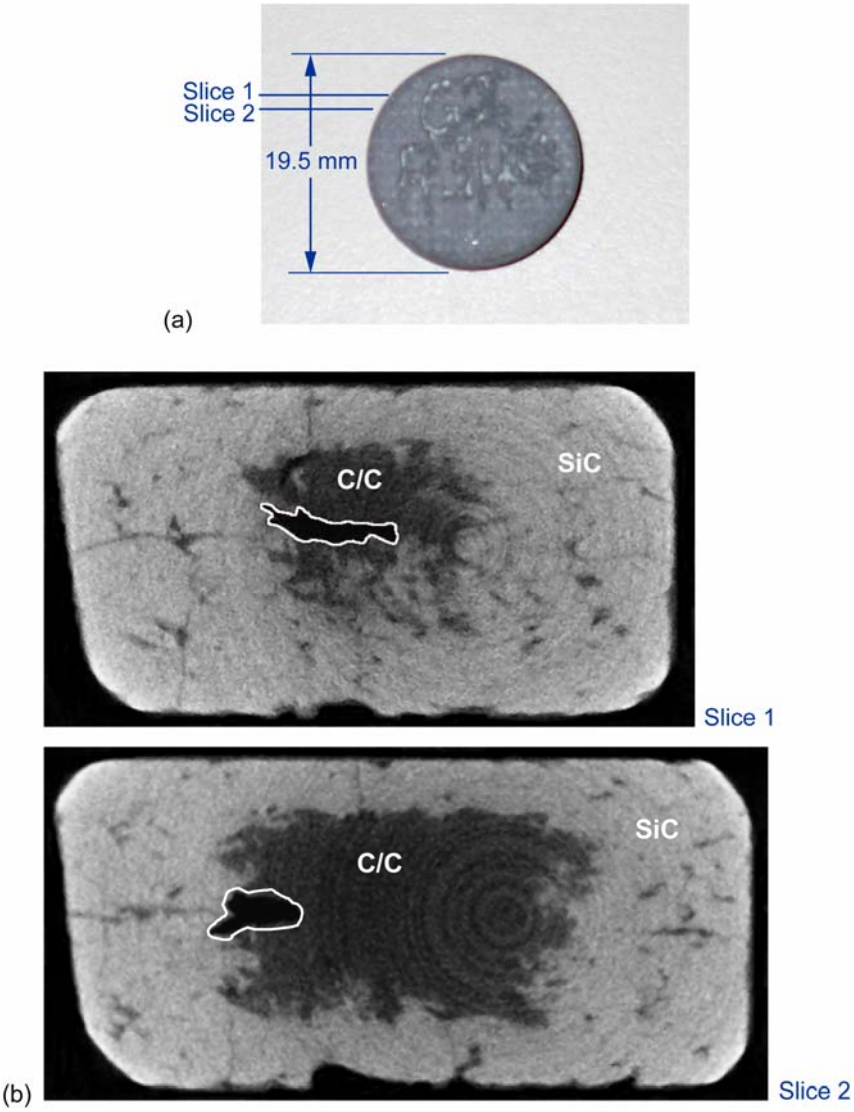

Figure 13.—X-ray computed tomography (CT) of SiC-coated RCC oxidized for 2.5 h in air at 1143 °C. (a) Location of CT slices. (b) Two CT slices.

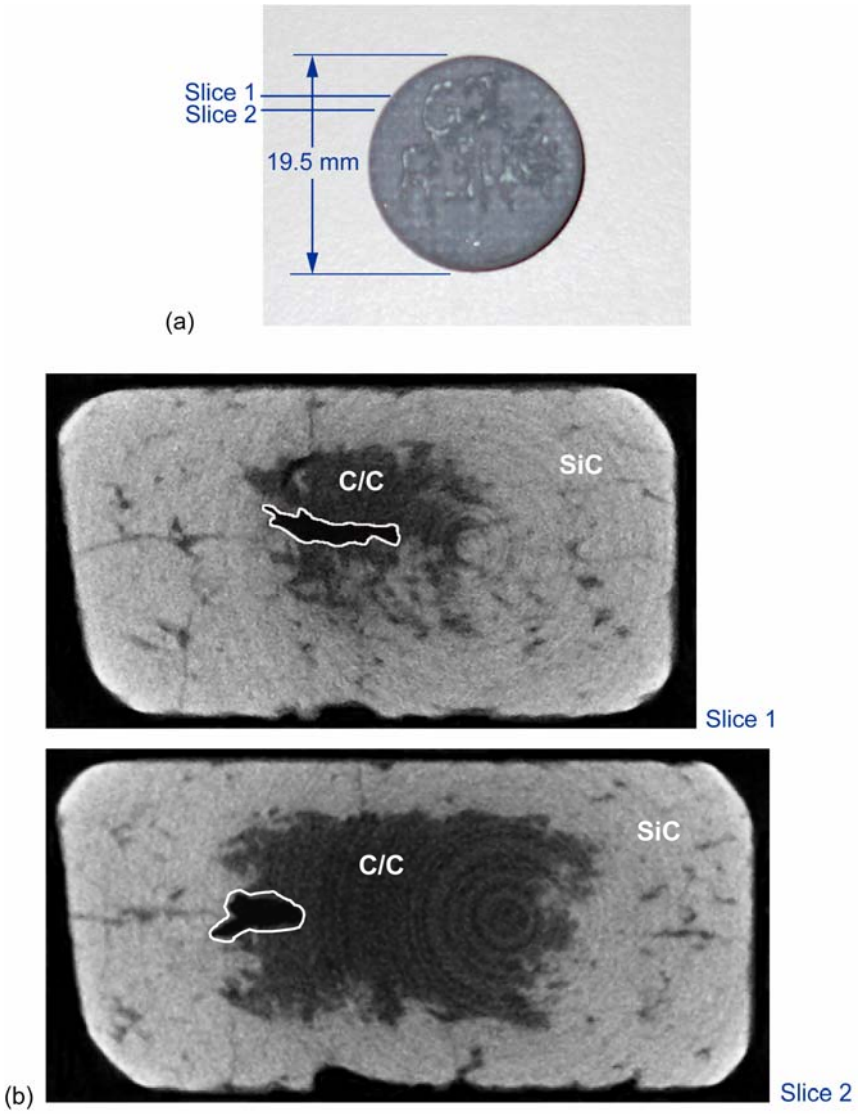

Figure 13.—Computed tomography (CT) of craze crack of SiC-coated RCC oxidized for 2.5 h in air at 1143 °C. (a) Location of CT slices. (b) Two CT slices.

Conclusions

The kinetics of subsurface oxidation of SiC-protected reinforced carbon/carbon has been studied in the diffusion control regime (1000 to 1300 °C) in air. Specimens with machined slots in the SiC coating as well as specimens with natural occurring craze cracks in the SiC coating were tested. The geometry of these oxidation pathways was characterized with the aim of obtaining the exposed area of the carbon/carbon. For the craze cracks, crack closure due to shrinkage was considered. Oxidation of the SiC walls was shown to be negligible under the conditions of this study. Oxidation damage of the carbon/carbon was assessed with weight changes, CT scans, and optical microscopy of sections. The CT scans confirm the idealized half-cylinder shape of the oxidation cavity in the case of a slot. A two-step diffusion control model for carbon oxidation is adapted to describe the growth kinetics of this half cylinder. Oxidation rates were first measured for the well-defined geometry of the slotted specimens. In the case of optical measurements of oxidation, the error associated with the predicted values of oxidation rate were primarily due to uncertainty in the measurements of the slot width, and the error in the measured rate values were due to uncertainty in measuring the size of the oxidation cavities. For these

optical measurements, measured rates were consistently lower than the predicted by a factor ranging from 0.45 to 0.62. For the weight loss measurements of oxidation, errors in the predictions were primarily due to errors in measuring the slot depth (coating thickness) and errors in the measurements were due to errors in measuring the slot width and length. Most of the predictions were within experimental error of the measurements, except for the largest slots (~1 mm width), where the measurements differ by a factor of ~0.33 from the predictions. Proceeding next to the actual craze cracks, the oxidation cavity was found to be highly irregular and approximated by a half-cylinder shape. Weight loss was used to measure oxidation, and again, errors in the predictions were primarily due to errors in measuring the slot depth (coating thickness) and errors in the measurements were due to errors in measuring the crack width and length. For oxidation below craze cracks, the predictions are generally within the experimental error of the measurements.

References

1. Curry, D.M.; Latchem, J.W.; and Whisenhunt, G.B.: Space Shuttle Orbiter Leading Edge Structural Subsystem Development. AIAA–1983–483, 1983.
2. Yurgartis, S.W.; Bush, M.D.; and Mast, B.E.: Morphological Description of Coating Cracks in SiC Coated Carbon-Carbon Composites. Surf. Coat. Tech., vol. 70, no. 1, 1994, pp. 131–142.
3. Buchanan, F.J.; and Little, J.A.: The Influence of Chemical Vapor-Deposition Conditions on the Structural Stability and Cracking of Silicon-Carbide Coatings on Carbon Carbon Composites. Surf. Coat. Tech., vol. 53, no. 2, 1992, pp. 137–146.
4. Jacobson, N.S.; and Curry, D.M.: Oxidation Microstructure Studies of Reinforced Carbon/Carbon. Carbon, vol. 44, no. 7, 2006, pp. 1142–1150.
5. Glime, W.H.; and Cawley, J.D.: Oxidation of Carbon-Fibers and Films in Ceramic-Matrix Composites—A Weak-Link Process. Carbon, vol. 33, no. 8, 1995, pp. 1053–1060.
6. Medford, J.E.: Prediction of Oxidation Performance of Reinforced Carbon-Carbon Material for Space Shuttle Leading Edges. AIAA–1975–730, 1975.
7. Bernstein, J.; and Koger, T.B.: Carbon-Film Oxidation-Undercut Kinetics. Electrochem. Soc., vol. 135, no. 8, 1988, pp. 2086–2090.
8. Courtright, E.L., et al.: Oxidation of Hafnium Carbide and Hafnium Carbide With Additions of Tantalum and Praseodymium. Oxid. Met., vol. 36, nos. 5–6, 1991, pp. 423–437.
9. Filipuzzi, L., et al.: Oxidation Mechanisms and Kinetics of 1D-SiC/C/SiC Composite Materials: I, An Experimental Approach. J. Am. Ceram. Soc., vol. 77, no. 2, 1994, pp. 459–466.
10. Filipuzzi, L.; and Naslain, R.: Oxidation Mechanisms and Kinetics of ID–SiC/C/SiC Composite Materials: II. Modeling. J. Am. Ceram. Soc., vol. 77, no. 2, 1994, pp. 467–480.
11. Holcomb, G.R.: Countercurrent Gaseous Diffusion Model of Oxidation Through a Porous Coating. Corrosion, vol. 52, no. 7, 1996, pp. 531–539.
12. Jacobson, N.S., et al.: Oxidative Attack of Carbon/Carbon Substrates Through Coating Pinholes. Carbon, vol. 37, no. 3, 1999, pp. 411–419.
13. Geiger, G.H.; and Poirier, D.R.: Transport Phenomena in Metallurgy. Addison-Wesley, Reading, MA, 1973, p. 464.
14. Svehla, R.A.: Estimated Viscosities and Thermal Conductivities of Gases at High Temperatures. NASA TR–R-132, 1962.
15. Sherwood, T.K.; Pigford, R.L.; and Wilke, C.R.: Mass Transfer. McGraw-Hill, New York, NY, 1975, p. 20.
16. Geankoplis, C.J.: Mass Transport Phenomena. Ohio State University Bookstores, Columbus, OH, 1984, p. 152.
17. Hewitt, G.W.: Gaseous Mass Transport Within Graphite. Chemistry and Physics of Carbon, Ch. Two, Philip L. Walker, Jr., ed., Marcel Dekker, New York, NY, 1965, pp. 73–120.
18. Margrave, John L.: Characterization of High Temperature Vapors. Wiley, New York, NY, 1967, p. 126.

19. Geiger, G.H.; and Poirier, D.R.: Transport Phenomena in Metallurgy. Addison-Wesley, Reading, MA, 1973, p. 468.
20. Williams, S.D., et al.: Ablation Analysis of the Shuttle Orbiter Oxidation Protected Reinforced Carbon-Carbon. J. Thermophys. Heat Transfer, vol. 9, no. 3, 1995, pp. 478–485.
21. Touloukian, Y.S., et al.: Thermal Expansion Nonmetallic Solids. Thermophysical Properties of Matter, Vol. 13, IFI/Plenum, New York, NY, 1977, p. 873.
22. Ullmann, T., et al.: Oxidation Protection of C/SiC Composites. Proceedings of 8th International Symposium on Materials in a Space Environment, Archachon, Frankreich, June 2000.
23. Ogbuji, L.U.J.T.; and Opila, E.J.: A Comparison of the Oxidation-Kinetics of SiC and SI_3N_4. J. Electrochem. Soc., vol. 142, no. 3, 1995, pp. 925–930.
24. Jacobson, N.S.: Corrosion of Silicon-Based Ceramics in Combustion Environments. J. Am. Ceram., vol. 76, no. 1, 1993, pp. 3–28.
25. Roth, D.J., et al.: NDE for Characterizing Oxidation Damage in Reinforced Carbon-Carbon Used on the NASA Space Shuttle Thermal Protection System. Ceram. Eng. Sci. Proc., vol. 26, no. 2, 2006, pp. 133–141.
26. Tedmon, C.S., Jr.: The Effect of Oxide Volatilization on the Oxidation Kinetics of Cr and Fe-CR Alloys. J. Electrochem. Soc., vol. 113, 1966, p. 766.
27. Opila, E.J.; and Jacobson, N.S.: SiO(g) Formation From SiC in Mixed Oxidizing-Reducing Gases. Oxid. Met., vol. 44, nos. 5–6, 1995, pp. 527–544.

Appendix
Symbols

A	area of SiC for oxidation
A'	area of exposed carbon-carbon for oxidation
c	molar concentration
D	diffusivity
J	molar flux
k	rate constant (weight^2/(unit area)^2-time)
L	depth of crack or coating thickness
l	crack length
M	molecular weight (g/mol)
P	total pressure in atmospheres
q	pore radius
R	gas constant
r	radius of half-cylinder cavity
s	crack spacing
T	temperature
t	time
v	molar velocity
W	weight loss
w	crack width
x	depth of crack coordinate with origin at SiC/C-C interface
x_f	depth to CO/CO_2 (region II) and CO_2/O_2 (region I) boundary
σ	average collision diameter between species i and N_2 (angstroms)
Ω	collision integral
α	coefficient of thermal expansion

Subscripts:

f	indicates boundary of regions I and II
i	species
l	linear
P	processing
p	parabolic
T	total

Superscripts:

ave	average
eff	effective
K	Knudsen
L	indicates position L
ord	ordinary
0	indicates position 0
I	region I
II	region II
*	indicates position x_f

REPORT DOCUMENTATION PAGE	Form Approved OMB No. 0704-0188

1. REPORT DATE *(DD-MM-YYYY)*	2. REPORT TYPE	3. DATES COVERED *(From - To)*
13-06-2007	Technical Memorandum	

4. TITLE AND SUBTITLE
Oxidation Through Coating Cracks of SiC-Protected Carbon/Carbon

5a. CONTRACT NUMBER

5b. GRANT NUMBER

5c. PROGRAM ELEMENT NUMBER

6. AUTHOR(S)
Jacobson, Nathan, S.; Roth, Don, J.; Rauser, Richard, W.; Curry, Donald, M.

5d. PROJECT NUMBER

5e. TASK NUMBER

5f. WORK UNIT NUMBER
WBS 377816.06.03.02.08

7. PERFORMING ORGANIZATION NAME(S) AND ADDRESS(ES)
National Aeronautics and Space Administration
John H. Glenn Research Center at Lewis Field
Cleveland, Ohio 44135-3191

8. PERFORMING ORGANIZATION REPORT NUMBER
E-16047

9. SPONSORING/MONITORING AGENCY NAME(S) AND ADDRESS(ES)
National Aeronautics and Space Administration
Washington, DC 20546-0001

10. SPONSORING/MONITORS ACRONYM(S)
NASA

11. SPONSORING/MONITORING REPORT NUMBER
NASA/TM-2007-214834

12. DISTRIBUTION/AVAILABILITY STATEMENT
Unclassified-Unlimited
Subject Category: 24
Available electronically at http://gltrs.grc.nasa.gov
This publication is available from the NASA Center for AeroSpace Information, 301-621-0390

13. SUPPLEMENTARY NOTES
Submitted to the Journal of Materials Science

14. ABSTRACT
The oxidation of SiC-protected carbon/carbon through machined slots and naturally occurring craze cracks in the SiC was studied. The slot and crack geometries were characterized, and the subsurface oxidation of the carbon/carbon substrate at temperatures of 1000 to 1300 °C in air was assessed using weight change, x-ray computed tomography, and optical microscopy of sections. Rate constants were derived from these measurements and compared with a two-step diffusion control model of carbon oxidation. Oxidation kinetic measurements on both the specimens with machined slots and with naturally occurring craze cracks showed good agreement with the model.

15. SUBJECT TERMS
Carbon/carbon; Oxidation

16. SECURITY CLASSIFICATION OF:			17. LIMITATION OF ABSTRACT	18. NUMBER OF PAGES	19a. NAME OF RESPONSIBLE PERSON
a. REPORT	b. ABSTRACT	c. THIS PAGE			Nathan S. Jacobson
U	U	U		27	19b. TELEPHONE NUMBER *(include area code)* 216-433-5498